Bi-allelic Truncating Mutations in *CEP78*, Encoding Centrosomal Protein 78, Cause Cone-Rod Degeneration with Sensorineural Hearing Loss

Prasanthi Namburi,[1] Rinki Ratnapriya,[2] Samer Khateb,[1] Csilla H. Lazar,[2,3] Yael Kinarty,[1,4] Alexey Obolensky,[1] Inbar Erdinest,[1] Devorah Marks-Ohana,[1] Eran Pras,[5,6] Tamar Ben-Yosef,[7] Hadas Newman,[6,8] Menachem Gross,[9] Anand Swaroop,[2,10] Eyal Banin,[1,10,*] and Dror Sharon[1,10,*]

Inherited retinal diseases (IRDs) are a diverse group of genetically and clinically heterogeneous retinal abnormalities. The present study was designed to identify genetic defects in individuals with an uncommon combination of autosomal recessive progressive cone-rod degeneration accompanied by sensorineural hearing loss (arCRD-SNHL). Homozygosity mapping followed by whole-exome sequencing (WES) and founder mutation screening revealed two truncating rare variants (c.893-1G>A and c.534delT) in *CEP78*, which encodes centrosomal protein 78, in six individuals of Jewish ancestry with CRD and SNHL. RT-PCR analysis of *CEP78* in blood leukocytes of affected individuals revealed that the c.893-1G>A mutation causes exon 7 skipping leading to deletion of 65bp, predicted to result in a frameshift and therefore a truncated protein (p.Asp298Valfs*17). RT-PCR analysis of 17 human tissues demonstrated ubiquitous expression of different *CEP78* transcripts. RNA-seq analysis revealed three transcripts in the human retina and relatively higher expression in S-cone-like photoreceptors of *Nrl*-knockout retina compared to rods. Immunohistochemistry studies in the human retina showed intense labeling of cone inner segments compared to rods. CEP78 was reported previously to interact with c-nap1, encoded by *CEP250* that we reported earlier to cause atypical Usher syndrome. We conclude that truncating mutations in *CEP78* result in a phenotype involving both the visual and auditory systems but different from typical Usher syndrome.

Inherited retinal diseases (IRDs) are a broad and growing group of heterogeneous neurodegenerative disorders[1,2] that can be either stationary or show progression with age primarily due to photoreceptor degeneration. IRD phenotypes are clinically distinguished by the onset of rod and cone involvement. The most common inherited retinal degeneration, retinitis pigmentosa (RP, MIM 268000) is characterized by a rod > cone pattern of dysfunction, accompanied by early impairment of night vision and progressive constriction of the visual fields, often leading to marked visual loss.[3] Cone-rod degeneration (CRD) is characterized by a cone > rod pattern, often exhibiting macular involvement and accompanied by loss of visual acuity, impairment of color vision, photophobia, and nystagmus in many cases.[4] The age of onset in CRD is variable, but most individuals demonstrate disease phenotype in the first two decades of life. Globally, RP is estimated to affect approximately 1 in about 3,500 individuals,[5–8] and we recently reported a higher prevalence of nonsyndromic RP in the vicinity of Jerusalem (~1:2,200).[9] The prevalence of CRD is much lower estimated as 1 in 40,000.[4] Both phenotypes are genetically heterogeneous (RetNet), with defects identified in pathways primarily involved in photoreceptor function including phototransduction, transcription and splicing, and intracellular trafficking.[10] As the photoreceptor outer segment is a modified cilium, mutations in genes associated with cilia biogenesis and transport cause pleiotropic ciliopathies with high penetrance of photoreceptor degeneration.[11–14]

About 10%–20% of individuals with RP suffer from Usher syndrome (USH) in which rod, followed by cone, degeneration is accompanied by sensorineural hearing loss (SNHL) and varying degrees of vestibular system involvement.[2,15–17] USH is a heterogeneous condition, both at the genetic and clinical levels, with mutations in at least 12 genes (see the databases RetNet and USHbases), historically classified into 3 main clinical sub-types. In recent years, a growing number of families with "atypical USH" were reported, but in all cases the symptoms related to rod photoreceptor involvement preceded cone degeneration.[18–21] The association of SNHL with CRD has not been previously reported.

In the present study, we used a combination of homozygosity mapping, whole-exome sequencing (WES), and founder mutation screening to identify the genetic cause of disease in families with the rare combination of CRD

[1]Department of Ophthalmology, Hadassah-Hebrew University Medical Center, Jerusalem, 91120, Israel; [2]Neurobiology-Neurodegeneration & Repair Laboratory, National Eye Institute, National Institutes of Health, Bethesda, MD, 20892-0610, USA; [3]Molecular Biology Center, Interdisciplinary Research Institute on Bio-Nano Sciences, Babes-Bolyai-University, 400271, Cluj-Napoca, Romania; [4]Department of Medical Neurobiology, Institute for Medical Research Israel-Canada, The Hebrew University-Hadassah Medical School, Jerusalem, 91120, Israel; [5]Department of Ophthalmology, Assaf Harofeh Medical Center, Zerifin, 70300, Israel; [6]Sackler Faculty of Medicine, Tel-Aviv University, Tel-Aviv, 6997801, Israel; [7]The Rappaport Faculty of Medicine, Technion-Israel Institute of Technology, Haifa, 3525433, Israel; [8]Department of Ophthalmology, Tel-Aviv Medical Center, Tel-Aviv, 64239, Israel; [9]Department of Otolaryngology-Head and Neck Surgery, Hadassah-Hebrew University Medical Center, Jerusalem, 91120, Israel
[10]These authors contributed equally to this work
*Correspondence: banine@cc.huji.ac.il (E.B.), dror.sharon1@gmail.com (D.S.)
http://dx.doi.org/10.1016/j.ajhg.2016.07.010.

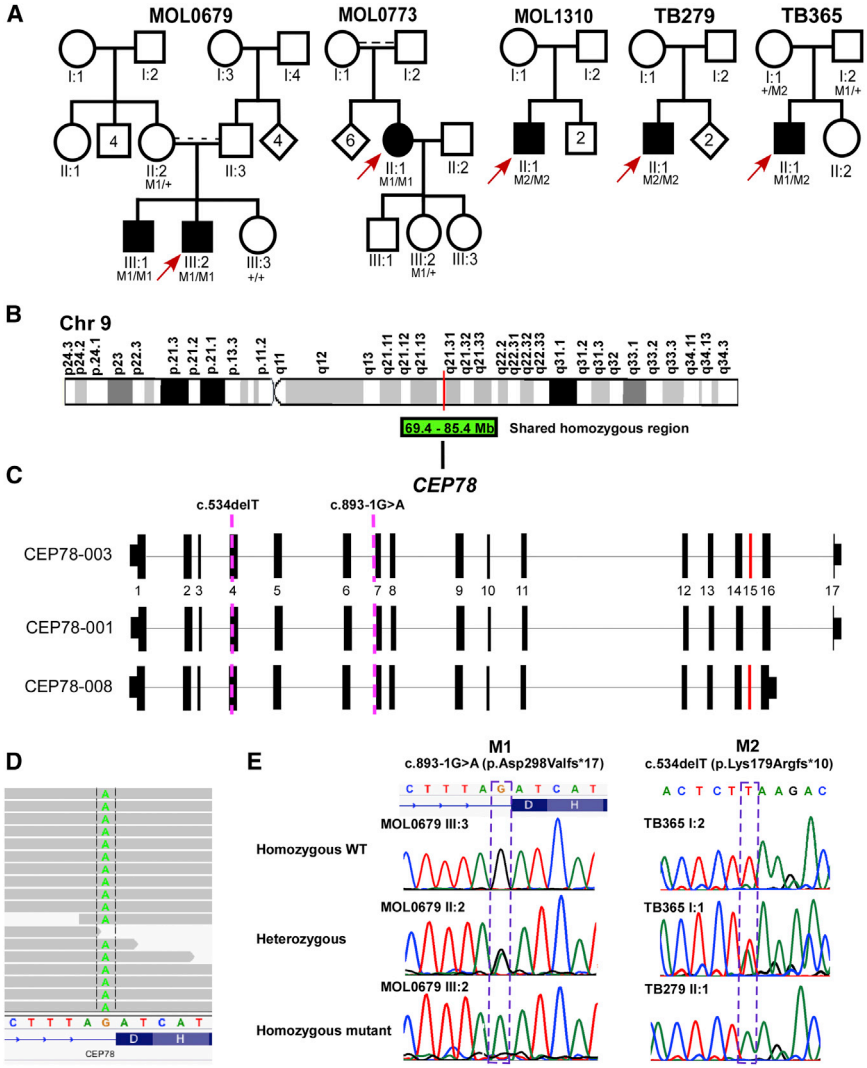

Figure 1. *CEP78* Genomic Arrangement and Mutation Identification

(A) Pedigree of families with *CEP78* mutation. Filled symbols designate affected individuals. Red arrows represent index case. Family number is depicted above each family tree and individual number below each symbol. The *CEP78* genotype of recruited individuals is depicted below the individual number: M1, c.893-1G>A; M2, c.534delT; +, wild-type allele. Genomic DNA was isolated using Maxwell® 16 Blood DNA Purification Kit (Promega).

(B) The chromosomal region harboring *CEP78* at chromosome 9.

(C) Schematic representation of three different transcripts of *CEP78* and the location of the identified mutations (pink dashed line). Black rectangles represent constitutive exons and red represent an alternatively-spliced exon.

(D) Exome sequence alignment of the c.893-1G>A mutation region in MOL0679 III:1. WES analysis was performed using Nextera Rapid Capture Expanded Exome kit on a HiSeq2500 platform (Illumina). Mapping to the human reference sequence (hg19, GRCH37) was performed using BWA, variants were called using GATK pipeline, and annotation of variants was done with ANNOVAR. Only a representative set of reads is depicted.

(E) Chromatograms of a homozygous wild-type (top), a heterozygous unaffected family member (middle), and a homozygous affected individual (bottom).

and SNHL inherited in an autosomal recessive (AR) mode. The tenets of the Declaration of Helsinki were followed, the study was approved by the Institutional Review Board (IRB), and prior to donation of a blood sample, informed consent was obtained from all participants. In our cohort of over 1,500 Israeli and Palestinian families with IRDs, six affected individuals from five families (Figure 1A) shared the same ethnicity (Jews of Iranian, Iraqi, or Afghani origin) and presented with a unique combination of CRD and SNHL. While some variability was present in the clinical manifestations between subjects (detailed case reports are provided in the Supplemental Note), a characteristic phenotype could be identified. All affected individuals presented with similar cone-dominated symptoms with a variable age of onset (ranging from 10 to 35 years) including photophobia, low visual acuity, impaired color vision, and visual field defects accompanied by SNHL, which also had a variable onset (ranging from 10 to 45 years). Electroretinographic (ERG) testing correlated with the visual symptoms, showing progressive loss of cone, followed by rod, photoreceptor function, in some cases accompanied by a reduced b/a wave ratio in the dark-adapted state (Table 1). Electrooculography (EOG) testing was performed in four affected individuals, and the Arden ratio was found to be reduced (Table 1), probably being secondary to photoreceptor degeneration. Funduscopic findings were characterized by the presence of prominent retinal atrophy along the major vascular arcades surrounding the macula that tended to expand at older ages. In addition, mild macular retinal pigment epithelium (RPE) changes and subtle peripheral salt and pepper changes were evident, with no bone-spicule-like pigmentation (BSP) (Figure 2). Characteristic ring-shaped atrophy was clearly evident on fundus autofluorescence (FAF) imaging, manifesting as a hypo-autofluorescent band along the vascular arcades surrounded by hyper-autofluorescent borders (Figure 2, right panels). In the three individuals who had visual acuity that permitted performance of color vision testing, none of the panels on the Ishihara 38-plate test were identified, and multiple errors with non-specific axes were present using the Farnsworth-Munsell D-15 test. Audiometry tests revealed bilateral SNHL affecting the middle frequencies, high frequencies, or both (Figure S1 and Table 1). One of the

Table 1. Clinical Data of Individuals with Bi-allelic *CEP78* Mutations

Individual Number (age in years)[a]	Genotype	Onset (years) of Visual Impairment	Best Corrected Visual Acuity (age)[a]	Refraction (age)[a]	Full Field ERG Results			EOG (%)	Hearing Impairment	
					30Hz Cone Flicker Amp/IT (age)*	Mixed Cone-Rod Response (age)*	Rod Response (age)*		Onset (years)	Frequencies
MOL0679 III:1 (37)	c.893-1G>A / c.893-1G>A	10	0.08 0.08 (44)	−3.00	ND ND (44)	a = 172, b = 175 a = 50, b = 43 (44)	110 47 (44)	122 (44)	45	High
MOL0679 III:2 (30)	c.893-1G>A / c.893-1G>A	10	0.15 LP (47)	−0.25 (47)	ND	ND	ND	NA	11	Medium and high
MOL0773 II:1 (29)	c.893-1G>A / c.893-1G>A	20	0.08 FC 1 m (43) FC 1 m (47)	−2.50 −1.25 (48) (48)	NA 25/42 (33) 15/43 (43) ND (48)	a = 127, b = 287 a = 91, b = 229 (33) a = 65, b = 94 (43) ND (48)	180 75 (33) ND (43) ND (48)	135 131 (47)	42	Bilateral flat curve
MOL1310 II:1 (38)	c.534delT / c.534delT	35	0.4	−8.25	NA	NA	NA	NA	36	NA
TB279 II:1 (47)	c.534delT / c.534delT	30	0.02	plano	ND	a = 41, b = 31	4	101	20	Medium and high
TB365 II:1 (38)	c.893-1G>A / c.534delT	28	0.12	−2.50	20 (38)	a = 134, b = 91	4	98	10	Medium and high

ND, nondetectable; NA, not available; Data represent average between both eyes. Best-corrected visual acuity is given as ratio; when below 0.05, Finger Counting (FC) is provided in meters; LP, light perception; Refraction is given as mean spherical equivalent of both eyes, in diopters.

Full-field Electroretinography (ERG) results include the following details: Light-adapted (LA) cone flicker amplitude (normal 60– 144 μV) and implicit time (IT, normal 27–33 ms); Dark-adapted (DA) rod response b-wave amplitude (normal range 200–500 μV); Dark-adapted mixed cone-rod a- and b-wave amplitudes (normal a-wave 90–350 μV, normal b-wave 380–630 μV).

Tel Aviv Sourasky Medical Center ERG normal ranges (applicable to individuals TB279 II:1 and TB365 II:1): LA cone flicker amplitude (65-190 μV) and implicit time (IT, msec, normal 24-30); DA rod response b-wave amplitude (normal 60-250 μV); Dark-adapted mixed cone-rod a- and b-wave amplitudes (normal a-wave 80–340 μV, normal b-wave 260–600 μV).

[a]The age at the first ERG testing is in parenthesis. Clinical tests performed at a different age are marked in parenthesis in the appropriate column.

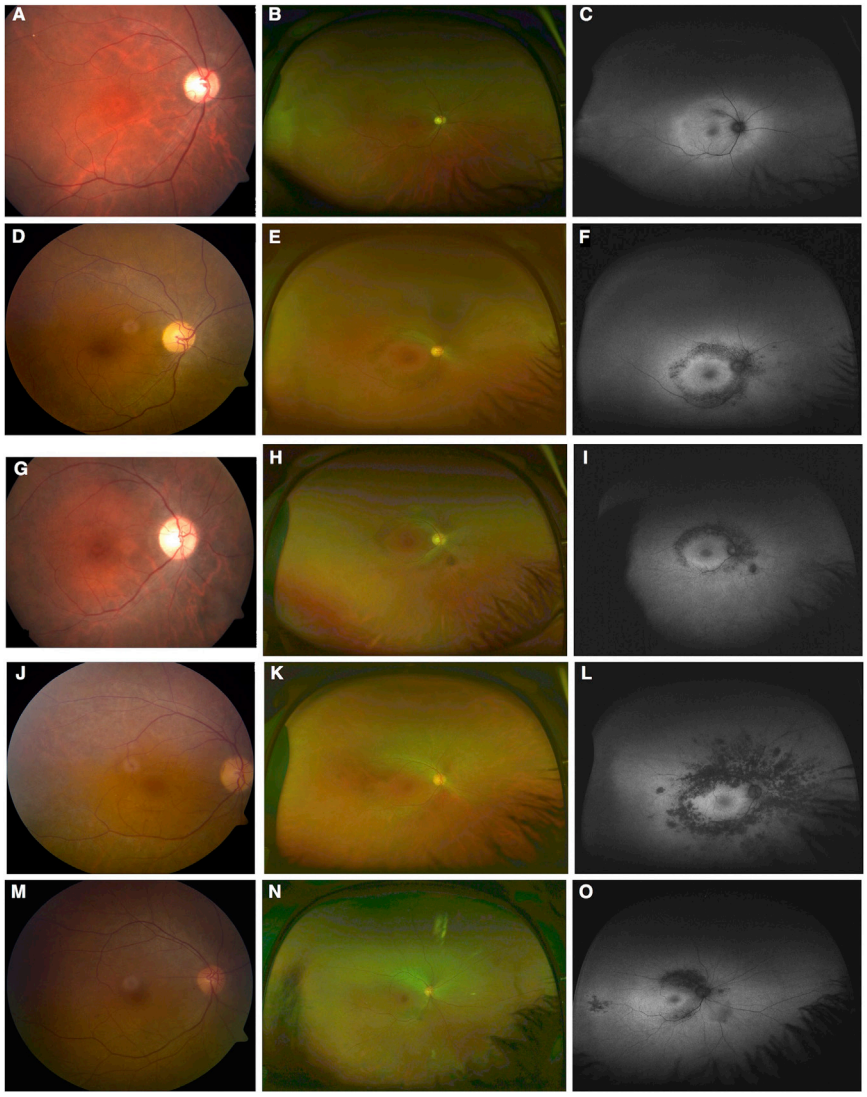

Figure 2. Imaging of Individuals with Biallelic *CEP78* Variants Ordered by Age
(A–C) TB365 II:1 (38 years).
(D–F) MOL0679 III:1 (44 years), (G–I) TB279 II:1 (47 years), (J–L) MOL0679 III:2 (47 years), and (M–O) MOL0773 II:1 (48 years). Color fundus photos of the posterior pole (left panels) and Optos wide-angle images (middle panels) show mild macular RPE changes, ring of atrophy along the vascular arcades surrounding the macula, and subtle peripheral salt and pepper changes with no BSPs. The findings are more clearly evident on fundus auto fluorescence (FAF) imaging (right panels) showing hypo-autofluorescence along the vascular arcades with a macular hyper-autofluorescent ring.

individuals, MOL0773 II:1, underwent audiometry at 47 years showing bilateral SNHL with a flat curve, involving all hearing frequencies (Figure S1C). Importantly, none of the affected individuals reported significant abnormalities of the vestibular system (detailed in Supplemental Note).

Aiming to identify the cause of disease in family MOL0679, in which the parents are distantly related, we performed homozygosity mapping on genomic DNA sample of the index case (III:2; Figure S2). Two large homozygous regions passed the analysis criteria: a very large region of 65.6 Mb on chromosome 9 (ranging from 19.8 to 85.4 Mb in reference sequence hg19) flanked by SNP markers rs1857437 and rs728695, and a smaller region of 34 Mb on chromosome 19 (15.3 to 49.1 Mb) flanked by markers rs2366267 and rs1073653. These regions harbor 628 and 744 genes, respectively, but do not harbor any known IRD-associated gene. We therefore performed WES analysis on the DNA sample of MOL0679 III:1 that revealed 30,379 sequence variants. Because compound heterozygous mutations can be identified in consanguineous families, we initially inspected a set of all 226 known IRD-associated genes[22] and did not identify any putative pathogenic disease-causing mutations. Analysis of known polymorphic markers in the two above-mentioned homozygous regions showed that the two siblings shared only a single large homozygous region on chromosome 9 (spanning 16 Mb, ranging from 69.4 to 85.4 Mb [Figure 1B], flanked by SNP markers rs369854466 and rs728695). We then performed detailed analysis of this homozygous region and identified 15 homozygous variants (Table S1), three of which were rare variants (minor allele frequency [MAF] $<$ 0.005) that are predicted to affect the amino-acid sequence of the corresponding gene. Two of the variants were missense that are predicted to be benign by the online prediction tools (PolyPhen 2, SIFT, and MutationTaster). The remaining single variant was a homozygous transition (c.893-1G>A, Figure 1D) in the acceptor site of exon 7 of *CEP78* (Genbank: NM_032171.1 [Figures 1C and 1D]) with coverage of 43X that was verified by Sanger sequencing (Figure 1E) and co-segregated with the phenotype in the family. Exon 7 includes 65 nucleotides and skipping of this exon is expected to result in a frameshift mutation (c.893_957del; p.Asp298Valfs*17). The sequence variant was not found in public databases (including the Exome Aggregation Consortium [ExAC] Server [Cambridge, MA, 03/2016]) and in an in-house database of 408 Israeli exomes.

Aiming to study whether c.893-1G>A is a recurrent mutation, we screened the index cases of the four remaining families that had a similar phenotype (MOL0773, MOL1310, TB279, and TB365, Figure 1A) for this mutation. Two index cases harbored the rare variant: MOL0773 II:1 was homozygous and TB365 II:1 was

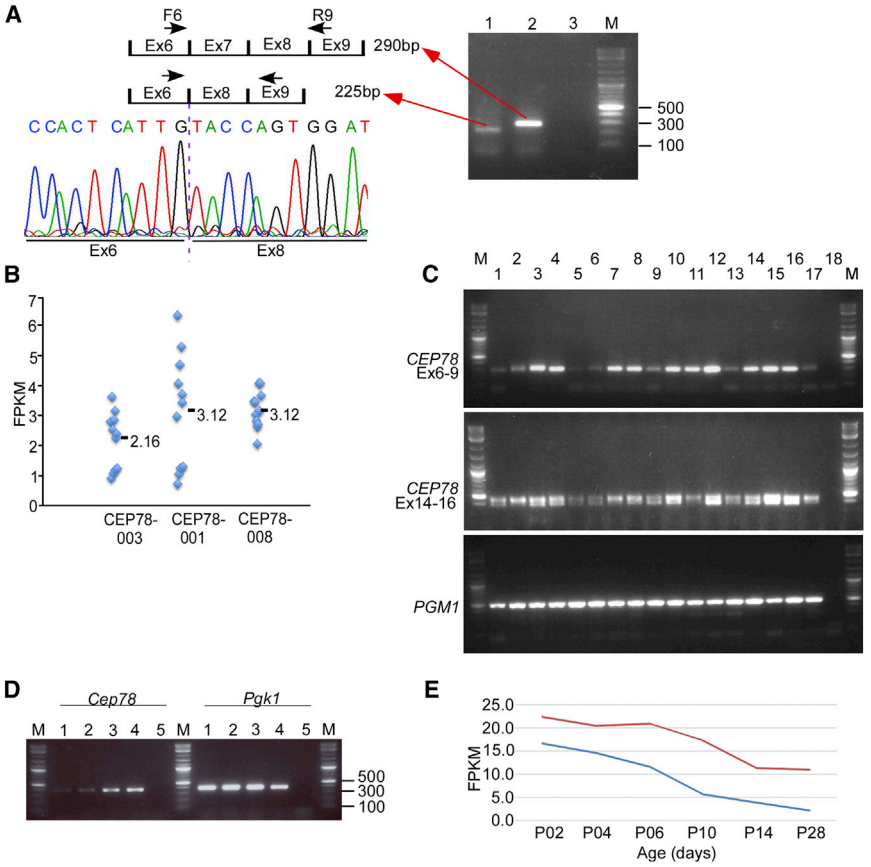

Figure 3. *CEP78* RNA Expression Analysis

(A) The effect of the c.893-1G>A mutation on *CEP78* mRNA splicing in blood leukocytes. RT-PCR analysis was performed on cDNA samples of a homozygous individual (MOL0773 II:1, lane 1) and a WT individual (lane 2). Lane 3 includes a negative control. M represents a 0.1–10 kb DNA ladder (100, 300, and 500 bp bands are indicated). The schematic drawing on the left represents the amplicons of the WT and mutant alleles as verified by direct Sanger sequencing. Total RNA was isolated using the QIAamp RNA Blood Mini Kit (QIAGEN) and RT-PCR was performed using Verso cDNA Kit (Thermo Scientific).

(B) RNaseq data extracted from 11 postmortem human retinal samples. The FPKM (fragments per kilobase of transcript per million mapped fragments) of the three identified *CEP78* transcripts is depicted. RNA was isolated with TRIzol LS and assessed using Bioanalyzer RNA 6000 Pico assay (Agilent Technologies). Strand-specific libraries were constructed with 20–100 ng of total RNA using TruSeq RNA Sample Prep Kit-v2 (Illumina). Reads were aligned to the Ensembl v73 transcriptome annotation using Bowtie2 and transcript quantitation was performed with eXpress.

(C) Expression level of *CEP78* versus *PGM1* (MIM 171900) in different human tissues (Clontech; cat #636643, lot No. 8101369A) using two sets of primers located in exons 6 through 9 and exons 14 through 16 and designed to amplify all three transcripts. Lane 1, bone marrow; 2, brain (whole); 3, fetal brain; 4, fetal liver; 5, heart; 6, kidney; 7, liver; 8, lung; 9, placenta; 10, prostate; 11, spleen; 12, thymus; 13, uterus; 14, small intestine; 15, spinal cord; 16, stomach; 17, retina; 18, negative control; and M, 0.1–10 kb DNA ladder.

(D) Expression of *Cep78* and *Pgk1* in the mouse retina (at the age of E14 [lane 1], P0 [lane 2], and P30 [lane 3]) and inner ear at P30 (lane 4). Negative controls are shown in lanes 5.

(E) RNA-seq analysis of *Cep78* in flow-sorted photoreceptors isolated from WT retina (blue) versus the cone-enriched Nrl-KO retina (red). GFP-positive cells were isolated from Nrlp-GFP or Nrlp-GFP;Nrl-KO mice retina at different postnatal stages of development by fluorescence-activated cell sorting (FACS).[30]

heterozygous. Sequencing analysis of the remaining exons in TB365 II:1 revealed an additional variant: a heterozygous deletion of thymidine in exon 4 (c.534delT), which is expected to cause a frameshift (p.Lys179Argfs*10). The two remaining index cases, MOL1310 II:1 and TB279 II:1, were found to be homozygous for c.534delT. In addition, we sequenced both exons 4 and 7, as well as flanking intronic sequences in 249 Eastern Jewish index cases with IRDs, but none of them carried either mutation or additional possible *CEP78* disease-causing mutation. Because both variants have been identified in individuals with a shared origin, we used a set of 21 SNP markers flanking *CEP78* to study whether c.893-1G>A and c.534delT are founder mutations (Table S2). Haplotype analysis revealed a shared and distinct haplotype for each mutation, covering homozygous regions of 6.3 and 11.3 Mb respectively, indicating that indeed, as expected, these are founder mutations in Jews originated from Iraq, Iran, and Afghanistan.

To study the effect of the c.893-1G>A mutation on splicing, we employed RT-PCR using RNA from blood leukocytes to amplify a fragment of *CEP78* mRNA. The primers we used are located in exons 6 and 9 (Table S3) and produced an expected 290 bp fragment in controls (Figure 3A) and a shorter 225 bp fragment in individuals who are homozygous for the mutation (Figure 3A, lane 1). Sanger sequencing of the mutant band revealed skipping of exon 7 leading to deletion of 65 nucleotides (Figure 3A, left panel). RT-PCR analysis of all available affected individuals and family members did not reveal significant differences in the abundance of the WT and the two mutant alleles (Figure S3), indicating that in leukocytes, short mutant CEP78 proteins that are likely to result in no protein function, are expected to be produced.

CEP78 includes 17 coding exons in the human genome spanning a genomic region of 31 Kb. To study the expression of *CEP78* in the human retina, we analyzed RNA-seq data of 11 individuals and identified three different protein-coding transcripts (Figures 1C and 3B). Analysis of retinal transcripts deposited in public databases show that exon 15 is an alternatively-spliced exon. In addition, we show here using RNA-seq analysis that transcripts

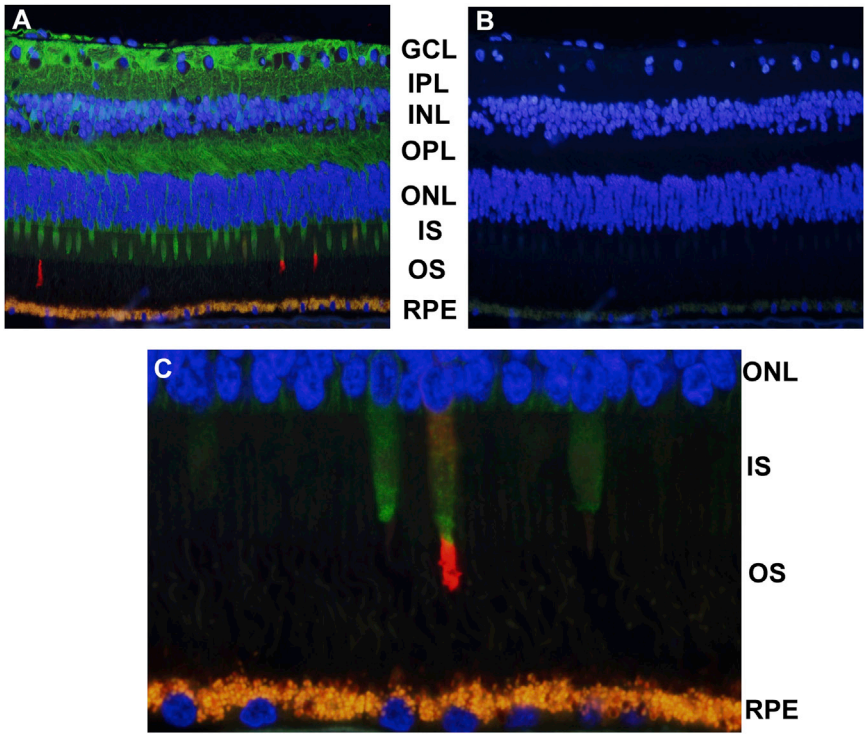

Figure 4. CEP78 Immunolocalization in the Human Retina

(A and B) Low-magnification images (20X) of control retina showing DAPI staining (B) and double staining (A) with the antibodies anti-CEP78 (HPA048846 from Sigma at a final concentration of 1:200) in green and anti-S-opsin (AB5407 from Chemicon International, Temecula; at a final concentration of 1:75) in red. The secondary antibodies were DyLight 488 donkey anti-rabbit and rhodamine red-X-conjugated donkey anti-goat IgG respectively (both in 1:250 dilution from Jackson Immuno Research Laboratories).

(C) Higher magnification of the photoreceptor-RPE region. Note dense staining of the cone inner segment and the base of the rod inner segment (original magnification 40X with digital zoom). GCL, ganglion cell layer; IPL, inner plexiform layer; INL, inner nuclear layer; OPL, outer plexiform layer; ONL, outer nuclear layer; IS, inner segments of photoreceptors; OS, outer segments of photoreceptors; RPE, retinal pigment epithelium layer.

including exon 17 (CEP78-001 and 003) are also expressed in the human retina (Figure 3B). All three transcripts show a similar level of expression with CEP78-003 the less common one (Figure 3B). Subsequent semiquantitative analysis of the distribution of *CEP78* transcripts in various human tissues revealed a ubiquitous and variable expression pattern (Figure 3C, upper two panels, and Figures S4A and S4B). In addition, the analysis revealed similar expression levels of transcripts including and lacking exon 15 in most studied tissues (Figure 3C, middle panel, and Figures S4B and S4D) with a relatively high expression level in the thymus. To study *Cep78* expression in the mouse retina, we used RT-PCR (followed by verification with Sanger sequencing) at different age points (embryonic day 14 [E14], postnatal day 0 [P0], and postnatal day 30 [P30]) in the WT mouse retina (Figures 3D, S4E, and Table S3). *Cep78* expression was evident at all time points with more intense amplification at P30 (Figures 3D and S4E). In addition, RT-PCR analysis of the inner ear shows robust amplification of *Cep78*, which is similar to that obtained in the retina (Figure S4E). To gain more insight on the expression level in specific retinal cells, we used RNA-seq to analyze the expression levels in flow-sorted photoreceptors of wild-type versus the *Nrl*-KO retina in mice (Figure 3E).[23] We observed a higher *Cep78* expression level in cones.

In all studied affected individuals, we observed a retinal phenotype showing initial and more pronounced cone dysfunction, which is followed and accompanied by less prominent rod involvement. This is reflected both in the symptoms experienced by the affected individuals (including decreased visual acuity, increased sensitivity to light and impaired color vision), in the funduscopic findings described above that mainly involve the posterior pole, and further substantiated by the ERG results that show a cone more than rod pattern of injury. Aiming to study the immunolocalization of CEP78 in the human retina, we performed immunohistochemistry studies with an anti-CEP78 antibody in sections of normal human (Figure 4) and mouse (Figure S5) retinas. The analysis revealed immunolocalization of CEP78 in many retinal cell types (Figure 4A compared to DAPI staining in Figure 4B). A similar immunolabeling retinal pattern was reported previously for FAM161A.[24] Intense staining of cone photoreceptor inner segments can be observed, while only weak labeling of the base of rod inner segments is evident (Figure 4C). These results are in-line with the observed retinal phenotype in which the cones are more affected than rods. IHC in the mouse retina (Figure S5) also revealed immunolocalization in various retinal cell-types including photoreceptor inner segments.

CEP78 orthologs can be found in mammals, amphibians, aves, fish, and insects. To gain insight into protein regions that are preserved along evolution, we performed a sliding window analysis calculating the mean amino-acid identity at a 30 amino-acid interval, comparing the human protein sequence to selected orthologs (Figure S6A). CEP78 contains a leucine-rich repeat (LRR) region, which is composed of 20–29 residue sequence motifs that are present in many proteins that participate in protein-protein interactions and have different functions and cellular locations. A limited level of amino-acid identity was found in the C terminus, while three regions show a relatively

high degree of preservation in all studied species: amino acids 178–287, which cover most of the LRR region, a sharp peak at amino acids 409–413, and a region between amino acids 511 and 566 (Figure S6A). Phylogeny analysis revealed, as expected, closely related sequences among mammalians and clear orthologous sequences in other species (Figure S6B). To compare the level of amino-acid preservation between CEP78 and 69 other IRD proteins (14 USH-related proteins and 55 arRP-related proteins listed in Table S4), we calculated the amino-acid identity levels between each human protein sequence and its orthologs in eight species (Figure S6C). The analysis indicates that CEP78 (red circle in Figure S6C) has an average level of preservation in most species along evolution.

Centrosomal protein 78kDa (CEP78) was previously shown to be localized to the human centrosome,[25] which is the major microtubule-organizing center of animal cells and through its influence on the cytoskeleton is involved in cell shape, polarity, and motility. The mother centriole determines the position of the flagella and cilia and becomes the basal body of these organelles.[26] The centrosome has also a crucial function in cell division because it determines the poles of the mitotic spindle that segregates duplicated chromosomes during cell division. CEP78 was reported previously to interact with another centrosomal protein, C-Nap1, encoded by *CEP250* (MIM 609689).[27] Interestingly, we reported previously that a null *CEP250* mutation causes atypical USH, characterized by early-onset SNHL, and a relatively mild RP phenotype.[21] Based on its cellular localization and interacting proteins, CEP78 is considered a ciliary protein.[28] Depletion of human CEP78 affects primary cilium assembly in RPE1 cells and decreased the proportion of ciliated cells up to 2-fold.[29]

Unlike all cases of retinal degeneration associated with SNHL (e.g., Usher syndrome) that were thus far reported, in which the retinal phenotype was typical RP, the individuals we describe here manifest ocular findings that are compatible with cone-rod degeneration. In line with the retinal phenotype, our immunohistochemistry analysis in the human retina shows more pronounced expression of *CEP78* in cones.

In summary, our results show that bi-allelic null variants in *CEP78* cause a syndrome that is characterized by CRD with SNHL, with relatively late onset of both ocular and hearing impairment. The funduscopic findings are characteristic, showing atrophy along the major vascular arcades that are best visualized using FAF imaging. To the best of our knowledge, this combined retinal and auditory phenotype has not been previously reported. The phenotype we describe here does not fall within the standard classification of Usher syndrome, and it should be noted that a relatively large number of affected individuals have been reported to suffer from "atypical" Usher syndrome with both retinal and hearing features that do not fit the three established Usher subtypes.[18–21] The results presented here further expand the spectrum of syndromes involving the auditory and visual systems that are due to defects in ciliary and/or centrosomal proteins.

Accession Numbers

The accession numbers for the c.893-1G>A and c.534delT variants reported in this paper were deposited in the Leiden open variation database (LOVD) with respective IDs 0000119346 and 0000119347.

Supplemental Data

Supplemental Data include six figures, four tables, and Supplemental Experimental Procedures and can be found with this article online at http://dx.doi.org/10.1016/j.ajhg.2016.07.010.

Acknowledgments

The authors thank all affected individuals and family members for their participation in this study. We are grateful to Lilach Binyamini and Shelly Stika for assistance in recruitment and clinical evaluation of the individuals and Alaa Abu-Diab for technical assistance. Whole-exome analysis utilized the computational resources of the NIH HPC Biowulf cluster. We thank Matthew Brooks, Jung-Woong Kim, Hyunjin Yang, and Ashley Walton for help with RNA-seq analysis. This research was supported by the United States – Israel Binational Science Foundation (grant number 2011202, to D.S. and A.S.), Foundation Fighting Blindness USA (BR-GE-0214-0639 to D.S., E.B., E.P., H.N., and T.B.-Y.), Israel Science Foundation (#2154/15 to S.K.), Chief Scientist office of the Israeli Ministry of Health and the Lirot association (#300009177 to S.K.), the Yedidut Research Grant (to E.B.), and the Intramural Research Program of the National Eye Institute, National Institutes of Health (to A.S.).

Received: March 17, 2016
Accepted: July 7, 2016
Published: September 1, 2016

Web Resources

ExAC Browser, http://exac.broadinstitute.org/
HomozygosityMapper software, http://www.homozygositymapper.org/
LOVD, http://www.lovd.nl/3.0/home
HPC @ NIH, http://hpc.nih.gov
OMIM, http://www.omim.org/
RetNet – Retinal Information Network, https://sph.uth.edu/retnet/home.htm
USHbases, https://grenada.lumc.nl/LOVD2/Usher_montpellier/USHbases.html

References

1. Rivolta, C., Sharon, D., DeAngelis, M.M., and Dryja, T.P. (2002). Retinitis pigmentosa and allied diseases: numerous diseases, genes, and inheritance patterns. Hum. Mol. Genet. *11*, 1219–1227.
2. Hartong, D.T., Berson, E.L., and Dryja, T.P. (2006). Retinitis pigmentosa. Lancet *368*, 1795–1809.
3. Berson, E.L. (1993). Retinitis pigmentosa. The Friedenwald Lecture. Invest. Ophthalmol. Vis. Sci. *34*, 1659–1676.

4. Hamel, C.P. (2007). Cone rod dystrophies. Orphanet J. Rare Dis. *2*, 7.
5. Bundey, S., and Crews, S.J. (1984). A study of retinitis pigmentosa in the City of Birmingham. II Clinical and genetic heterogeneity. J. Med. Genet. *21*, 421–428.
6. Bunker, C.H., Berson, E.L., Bromley, W.C., Hayes, R.P., and Roderick, T.H. (1984). Prevalence of retinitis pigmentosa in Maine. Am. J. Ophthalmol. *97*, 357–365.
7. Haim, M. (2002). Epidemiology of retinitis pigmentosa in Denmark. Acta Ophthalmol. Scand. Suppl. *233*, 1–34.
8. Rosenberg, T. (2003). Epidemiology of hereditary ocular disorders. Dev. Ophthalmol. *37*, 16–33.
9. Sharon, D., and Banin, E. (2015). Nonsyndromic retinitis pigmentosa is highly prevalent in the Jerusalem region with a high frequency of founder mutations. Mol. Vis. *21*, 783–792.
10. Veleri, S., Lazar, C.H., Chang, B., Sieving, P.A., Banin, E., and Swaroop, A. (2015). Biology and therapy of inherited retinal degenerative disease: insights from mouse models. Dis. Model. Mech. *8*, 109–129.
11. Valente, E.M., Rosti, R.O., Gibbs, E., and Gleeson, J.G. (2014). Primary cilia in neurodevelopmental disorders. Nat. Rev. Neurol. *10*, 27–36.
12. Rachel, R.A., Li, T., and Swaroop, A. (2012). Photoreceptor sensory cilia and ciliopathies: focus on CEP290, RPGR and their interacting proteins. Cilia *1*, 22.
13. Estrada-Cuzcano, A., Roepman, R., Cremers, F.P., den Hollander, A.I., and Mans, D.A. (2012). Non-syndromic retinal ciliopathies: translating gene discovery into therapy. Hum. Mol. Genet. *21* (R1), R111–R124.
14. Sorusch, N., Wunderlich, K., Bauss, K., Nagel-Wolfrum, K., and Wolfrum, U. (2014). Usher syndrome protein network functions in the retina and their relation to other retinal ciliopathies. Adv. Exp. Med. Biol. *801*, 527–533.
15. Rosenberg, T., Haim, M., Hauch, A.M., and Parving, A. (1997). The prevalence of Usher syndrome and other retinal dystrophy-hearing impairment associations. Clin. Genet. *51*, 314–321.
16. Keats, B.J., and Savas, S. (2004). Genetic heterogeneity in Usher syndrome. Am. J. Med. Genet. A. *130A*, 13–16.
17. Kimberling, W.J., Orten, D., and Pieke-Dahl, S. (2000). Genetic heterogeneity of Usher syndrome. Adv. Otorhinolaryngol. *56*, 11–18.
18. Bashir, R., Fatima, A., and Naz, S. (2010). A frameshift mutation in SANS results in atypical Usher syndrome. Clin. Genet. *78*, 601–603.
19. Kalay, E., de Brouwer, A.P., Caylan, R., Nabuurs, S.B., Wollnik, B., Karaguzel, A., Heister, J.G., Erdol, H., Cremers, F.P., Cremers, C.W., et al. (2005). A novel D458V mutation in the SANS PDZ binding motif causes atypical Usher syndrome. J. Mol. Med. *83*, 1025–1032.
20. Liu, X.Z., Hope, C., Walsh, J., Newton, V., Ke, X.M., Liang, C.Y., Xu, L.R., Zhou, J.M., Trump, D., Steel, K.P., et al. (1998). Mutations in the myosin VIIA gene cause a wide phenotypic spectrum, including atypical Usher syndrome. Am. J. Hum. Genet. *63*, 909–912.
21. Khateb, S., Zelinger, L., Mizrahi-Meissonnier, L., Ayuso, C., Koenekoop, R.K., Laxer, U., Gross, M., Banin, E., and Sharon, D. (2014). A homozygous nonsense CEP250 mutation combined with a heterozygous nonsense C2orf71 mutation is associated with atypical Usher syndrome. J. Med. Genet. *51*, 460–469.
22. Beryozkin, A., Shevah, E., Kimchi, A., Mizrahi-Meissonnier, L., Khateb, S., Ratnapriya, R., Lazar, C.H., Blumenfeld, A., Ben-Yosef, T., Hemo, Y., et al. (2015). Whole Exome Sequencing Reveals Mutations in Known Retinal Disease Genes in 33 out of 68 Israeli Families with Inherited Retinopathies. Sci. Rep. *5*, 13187.
23. Mears, A.J., Kondo, M., Swain, P.K., Takada, Y., Bush, R.A., Saunders, T.L., Sieving, P.A., and Swaroop, A. (2001). Nrl is required for rod photoreceptor development. Nat. Genet. *29*, 447–452.
24. Di Gioia, S.A., Letteboer, S.J., Kostic, C., Bandah-Rozenfeld, D., Hetterschijt, L., Sharon, D., Arsenijevic, Y., Roepman, R., and Rivolta, C. (2012). FAM161A, associated with retinitis pigmentosa, is a component of the cilia-basal body complex and interacts with proteins involved in ciliopathies. Hum. Mol. Genet. *21*, 5174–5184.
25. Andersen, J.S., Wilkinson, C.J., Mayor, T., Mortensen, P., Nigg, E.A., and Mann, M. (2003). Proteomic characterization of the human centrosome by protein correlation profiling. Nature *426*, 570–574.
26. Nigg, E.A., and Raff, J.W. (2009). Centrioles, centrosomes, and cilia in health and disease. Cell *139*, 663–678.
27. Fogeron, M.L., Müller, H., Schade, S., Dreher, F., Lehmann, V., Kühnel, A., Scholz, A.K., Kashofer, K., Zerck, A., Fauler, B., et al. (2013). LGALS3BP regulates centriole biogenesis and centrosome hypertrophy in cancer cells. Nat. Commun. *4*, 1531.
28. Brekman, A., Walters, M.S., Tilley, A.E., and Crystal, R.G. (2014). FOXJ1 prevents cilia growth inhibition by cigarette smoke in human airway epithelium in vitro. Am. J. Respir. Cell Mol. Biol. *51*, 688–700.
29. Azimzadeh, J., Wong, M.L., Downhour, D.M., Sánchez Alvarado, A., and Marshall, W.F. (2012). Centrosome loss in the evolution of planarians. Science *335*, 461–463.
30. Kim, J.-W., Yang, H.-J., Oel, A.P., Brooks, M.J., Jia, L., Li, W., Allison, W.T., and Swaroop, A. (2016). Recruitment of rod photoreceptors from short-wavelength-sensitive cones during the evolution of nocturnal vision in mammals. Dev. Cell *37*, 520–532.